

BIOMEDICAL PAPER

A potential function approach to surface coverage for a surgical robot

NATHAN ABRAHAM¹, ALON WOLF^{1,3}, & HOWIE CHOSET^{1,2}

¹The Robotics Institute, ²Department of Mechanical Engineering, Carnegie Mellon University, Pittsburgh, and ³Institute for Computer Assisted Orthopaedic Surgery, Western Pennsylvania Hospital, Pittsburgh, Pennsylvania, USA

(Received 7 September 2004; accepted 3 February 2005)

Abstract

This paper considers some implementation issues in a path planner for achieving uniform coverage of a non-Euclidean bony surface embedded in \mathbb{R}^3 space. The target application for this planner is bone removal in orthopaedic surgery, but the technique can also be applied to other general surface-coverage problems. Specifically, we use cellular decomposition and sweep lines to generate a set of meaningful way-points for the bone-burring robot to visit, then navigate between these way-points using potential functions.

Keywords: *Joint arthroscopy, medical robotics, surface coverage, potential functions*

Key link: <http://voronoi.sbp.ri.cmu.edu/mbars/>

Introduction

Medicine is a field where advances in technology can directly help increase the quality of life for humans. In the operating room alone, there are several systems currently available to aid in surgical procedures. With the assistance of computer-controlled robotic systems, procedures can be performed more accurately and less invasively [1,2]. Orthopaedic surgery is one such area where the field of robotics has been shown to be highly applicable. Procedures that require the precise reshaping of bone lend themselves to benefiting from highly accurate robots. Previous work in this field includes a force analysis of an orthopaedic tool [3], a semi-active robot to aid a surgeon [4], and a calibrated robot to actively participate in the surgery itself [5]. Several other commercially available platforms exist as well [6–9].

We present a new system that combines a medical robotic platform with techniques usually associated with mobile robot motion planning. By treating the

tip of the cutting tool as a mobile robot and the area of surgery as a free space, we can apply many techniques that have already been shown to be successful. Potential functions are one such approach. Potential functions are generally used to create a field where high potential areas correspond to obstacles in a space, while areas of low potential correspond to goals. Using a gradient descent algorithm, one can navigate to a goal. Cellular decomposition, a hierarchical tool in decomposing spaces, is another approach. Complex spaces are broken down into a set of cells that are easy to traverse. Using these tools, we aim to automate portions of orthopaedic surgeries.

This paper focuses on one specific facet of many orthopaedic surgeries that is also common to automation tasks in general: surface coverage. Several commonly performed orthopaedic surgeries require the use of a bone-milling device to reshape the surface of a bone so as to accommodate an implant. In fact, total knee arthroplasties alone represent

an annual cost upwards of \$11.2 billion. Any modification that increases a surgeon's accuracy will in turn save a significant amount of money. In this paper, we present an algorithm for automatically computing a trajectory for a bone-milling robot that covers the surface of a bone. Specifically, our algorithm combines cellular decomposition, sweep lines, and potential functions to generate a path that uniformly covers the surface.

Operation and requirements

The Miniature Bone-Attached Robotic System (MBARS) is a robust orthopaedic surgery robot. Specifically, MBARS is a Stewart-Gough platform with a commercial bone burr mounted on the upper platform (Figure 1). Three surgical pins rigidly attach the robot to the area of operation, making the bone surface and robot base act as a single rigid body. Next, using a point probe, the robot palpates the operational bone surface and collects surface points in the end-effector coordinate system. Contact with the bone surface is detected using the force feedback capability inherent in the robot's low-level controller; contact is indicated by a sudden increase in force. (If force feedback is not available, then one can connect the point probe to a force sensor which can be attached to the robot's end-effector.) This process results in a cloud of points in the robot coordinate system, and intra-operative planning is already performed in the robot (or tool) coordinate system. This has a significant benefit in that there are no relative motions between the knee and the robot, so there is no need for a dynamic tracking sensor to detect relative motion between the robot and the anatomy. Moreover, this approach also minimizes errors introduced during the registration process and in the resulting transformations between the robot's planner and anatomy coordinate systems. MBARS can achieve higher accuracy at a much lower cost.



Figure 1. CAD drawing of MBARS. [Color version available online]

The clinical study we chose to focus on is patellofemoral joint (PFJ) arthroplasty. In this surgery, a surgeon resects the patella (kneecap) and uses a bone-burring cutting tool to shape the patellofemoral surface. Through an iterative trial and error process, the bone is gradually shaved, and the trochlear component is placed in the newly formed cavity of the patellofemoral surface. Once the trochlear component is in place, an additional prosthesis is placed on the underside of the patella, thus reducing friction between the patella and patellofemoral surface and, consequently, reducing pain for the patient [10] (Figure 2).

MBARS will perform only the patellofemoral surface reshaping. To be able to achieve this task, the robot's workspace needs to encompass the entire volume of bone to be milled. A 5-cm³ operating space was chosen, as it safely contains the largest possible prosthesis for the operation.

An additional requirement for this task is the ability to match or surpass the accuracy of a surgeon's hand. Typical industrial robots are serial mechanisms: Linkages are aligned serially such that every joint is connected to exactly two linkages, and every linkage is connected to at most two joints. For example, the structure of a person's arm can be represented as a serial robot: the hand is connected to the torso through the wrist, elbow, and shoulder joints. A major drawback to these structures is that positional accuracy is compromised as more joints are added to the system.

Parallel mechanisms, however, do not have this problem. Linkages of parallel mechanisms are not constrained to be connected by only two joints,

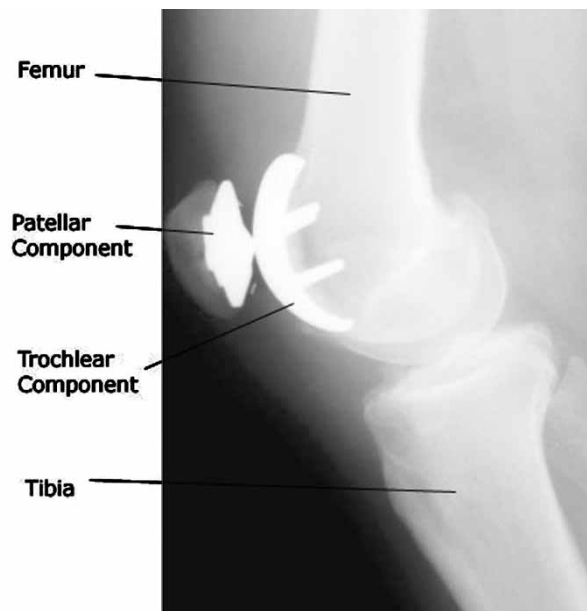


Figure 2. X-ray showing the final position of the implant [10].

but rather the end-effector of the robot is connected directly to its base through many linkages. Both loads on the system and positional error are mediated through the joints, thus allowing a stronger, more accurate robot. The drawback to these systems is the decreased workspace that results from non-serial connections. However, this can be advantageous for a surgical robot as the operational workspace is within the robot's effective workspace [11].

Implant fitting

A major requirement of the surgery is that both sides, as well as the distal tip, of the trochlear component

must lie flush with the patellofemoral surface so that the patellar component will not catch during joint movement [10]. Our goal is to find a final position for the implant prior to making any cuts in the bone. This requires surface models of both the implant and the knee, which we construct using CT imagery (Figure 3).

The surgery requires the centerline of the implant to lie along the trochlear groove of the knee to ensure proper alignment. Via software, a user (surgeon) marks the trochlear groove of the bone surface and the centerline of the implant in the corresponding computer models. The implant model is moved such that its centerline is coplanar with the patellofemoral centerline (Figure 4). A translation

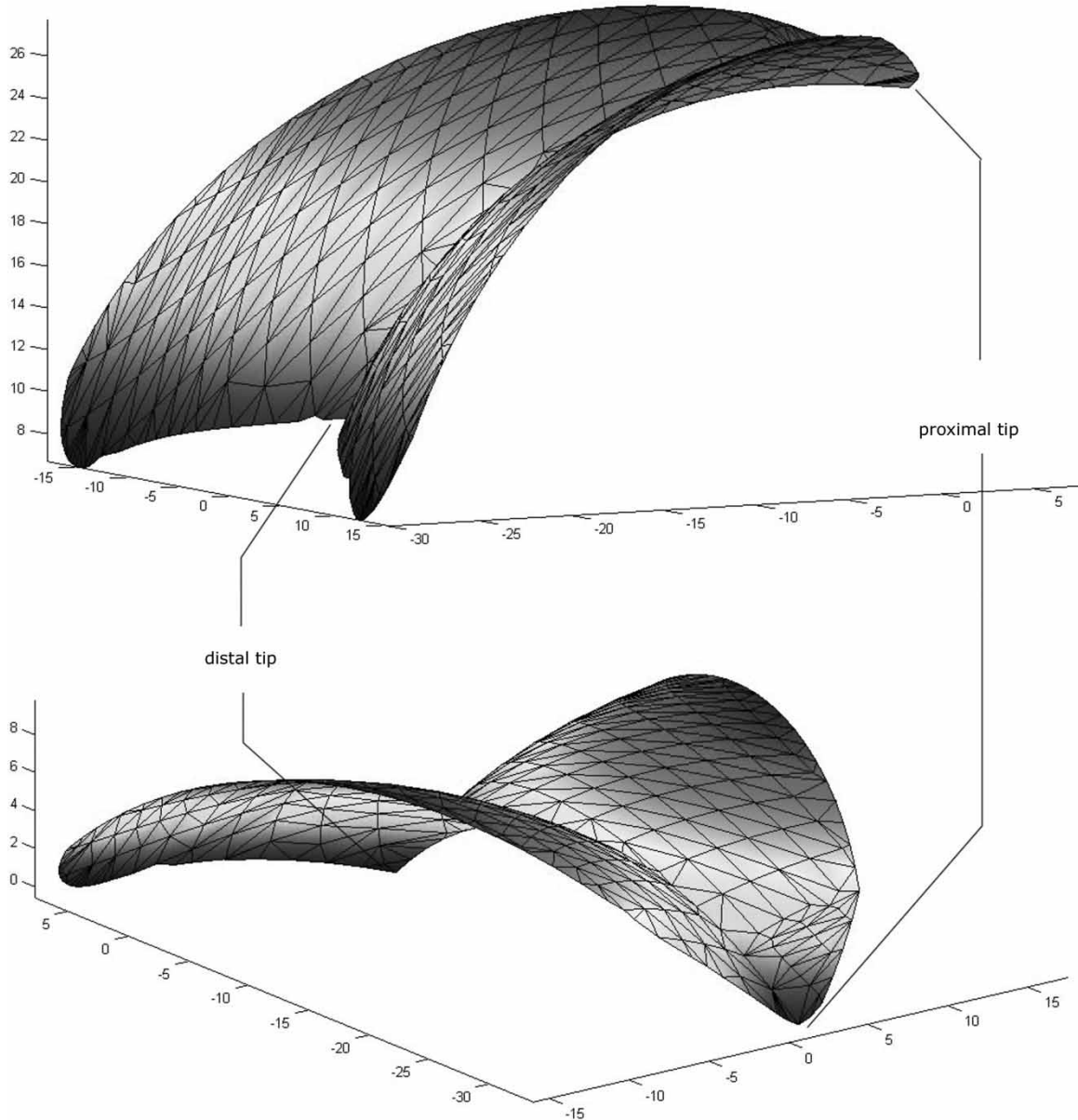


Figure 3. Two views of the trochlear component surface model. [Color version available online]

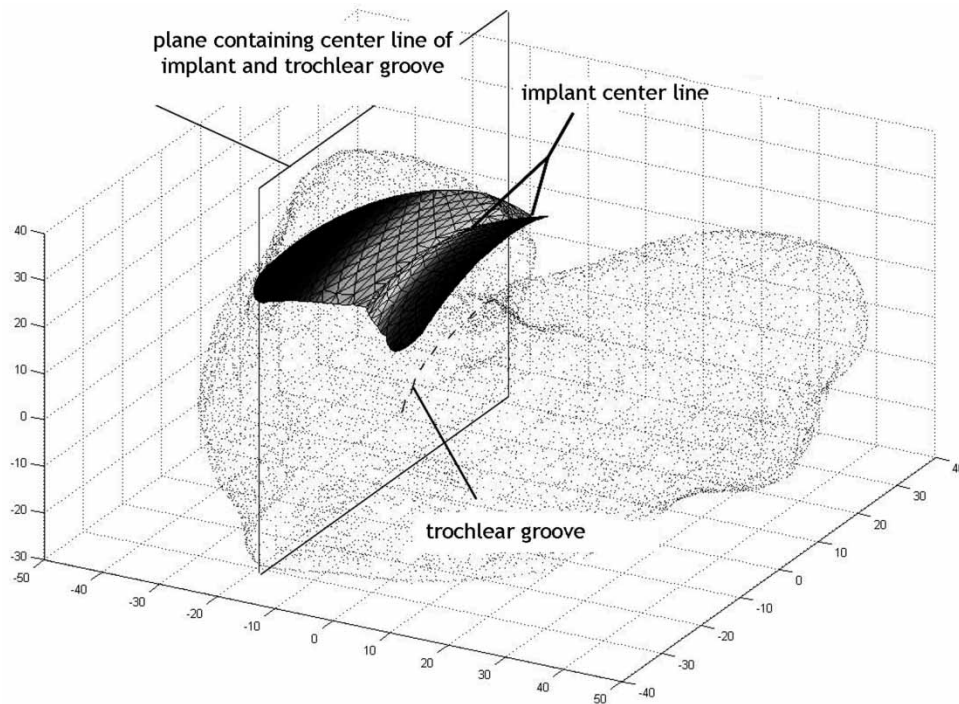


Figure 4. The implant aligned along the trochlear groove. The plane contains both the centerline of the implant and the trochlear groove of the knee model. Small dots represent each point of the knee collected by the CT imagery. [Color version available online]

to put the distal tip of the implant surface in contact with the knee is performed, then an exhaustive search for different orientations of the implant is conducted (Figure 5). The algorithm selects the rotation, $R(\theta)$,

about the lateral-medial axis of the trochlear component, I , which minimizes the distance between points on the implant component and their corresponding closest points on the patellofemoral

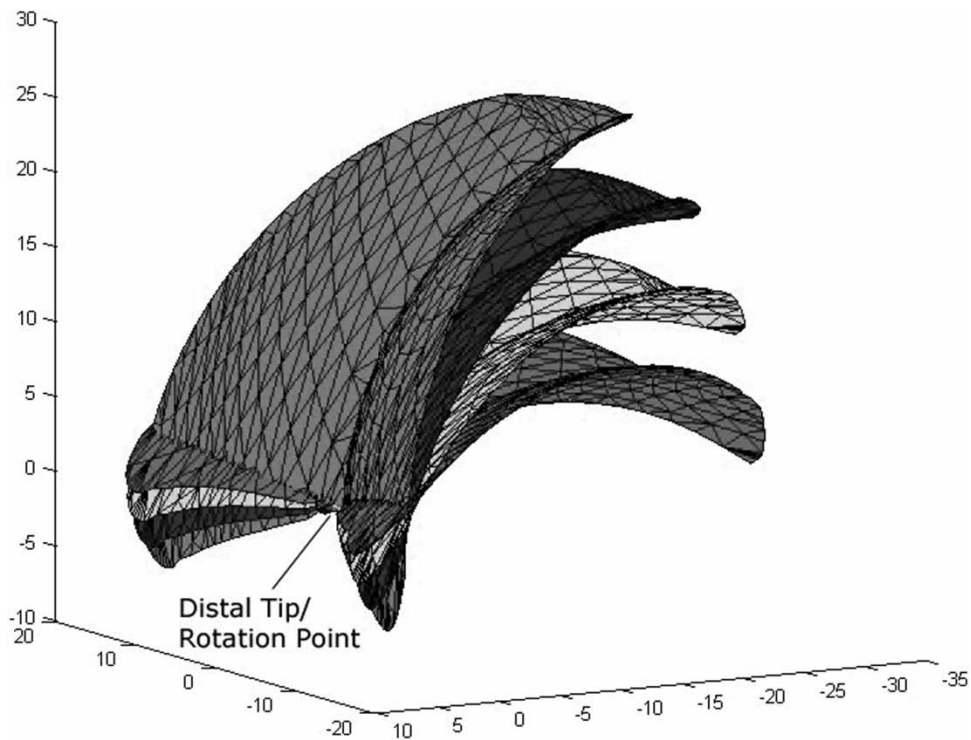


Figure 5. Implant in four positions rotated in 15° increments about the distal tip. [Color version available online]

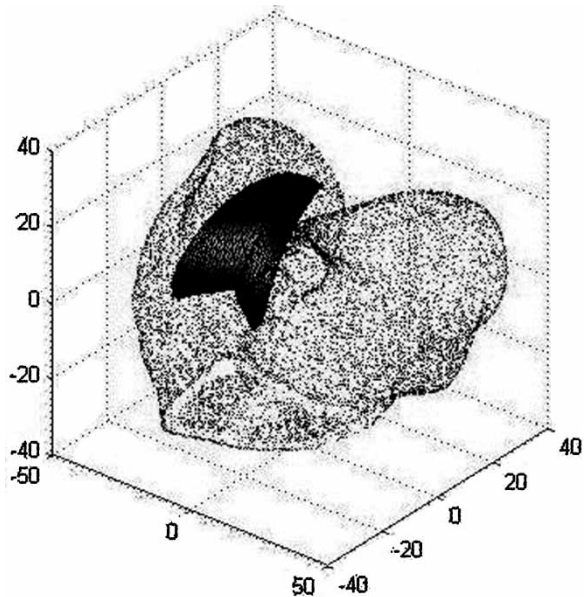


Figure 6. Implant fitted on patellofemoral surface. [Color version available online]

surface, S (Figure 6) (Equations 1 and 2).

$$I_R = I \cdot R(\theta) \quad (1)$$

$$\sum_j (I_{R,j} - S_j)^2 \quad (2)$$

The result of the completed algorithm is an accurate fit between the implant and the bone surface. However, as accurate as the results are, the surgeon retains the capability to refine and change the implant location based on his judgment and understanding. Once the surgeon approves the implant location, it is used as an input for the robot’s path-planning algorithm.

Sweep line and path planning

Once the implant position on the surface is determined, a trajectory is calculated for MBARS to achieve uniform coverage. To do this, we treat the bone burr tip as a mobile robot, or particle. Once the trajectory for the particle is calculated, inverse kinematics are used to find the configuration of the robot. Because MBARS is a parallel manipulator, inverse kinematics becomes a trivial problem of calculating link lengths [12].

For the task of coverage, we use cell decomposition, a technique for achieving complete coverage of connected free spaces. Using this technique, we break a space into a connected set of cells that are easily covered. Therefore, covering the entire space becomes an easily solved problem of visiting every

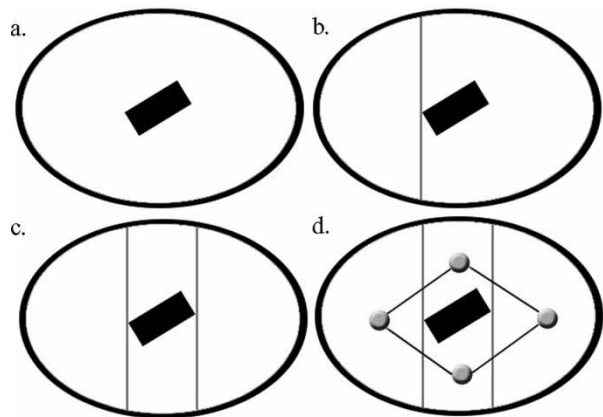


Figure 7. Cellular decomposition: the resulting cells, marked by circular icons, are shown in step d.

cell. In two-dimensional spaces, boustrophedon cell decomposition (one particular type of cell decomposition) is carried out by moving a scan line across a space and marking the points where the scan line changes continuity. These points mark where the border of a cell occurs [13]. Figure 7 shows the cellular decomposition of an example space as a scan line is moved from left to right. The cell decomposition of the implant from a scan line moving in the distal-proximal direction yields 3 cells (Figure 8).

Once we have the cells, we wish to generate a coverage path within each cell. We have chosen to use a simple back-and-forth pattern to achieve coverage (Figure 9), but we also need to regulate the distance between passes to ensure uniformity. To ensure a uniform surface of the bone after milling, equal

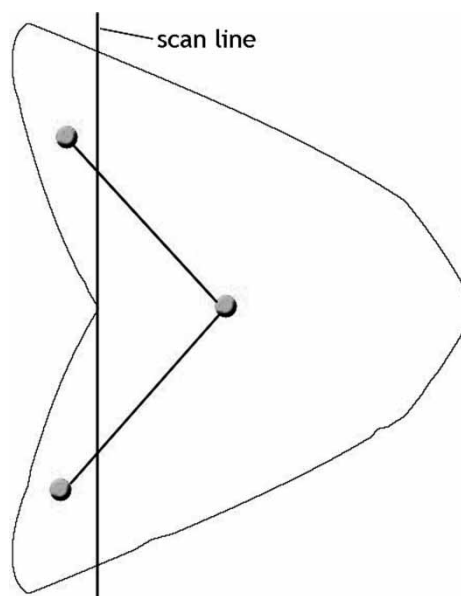


Figure 8. Cellular decomposition of the implant with the scan line shown at the critical step.

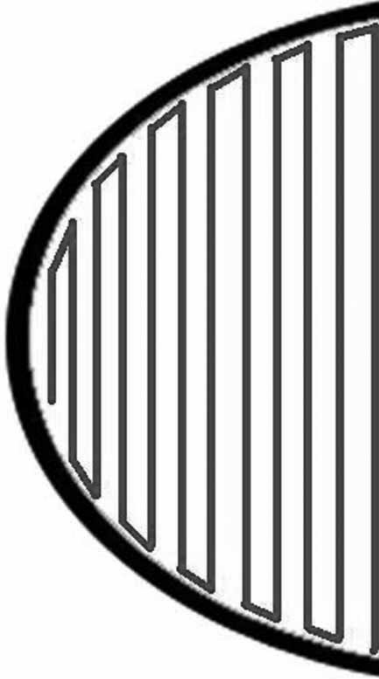


Figure 9. Coverage of the leftmost cell from figure 7.

sweeps of the burr must be made such that *scallop height*, i.e., the height of ridges on the surface, remains constant [14] (Figure 10). To do so, we use an approach as outlined in reference [15]. The algorithm works as follows:

1. Find the intersection of the knee model with a 2D plane. This intersection will be known as the *start curve*. For ease of implementation, choose the 2D plane such that the start curve will lie at one of the proximal/distal extremities of where the implant rests on the surface (either the proximal tip or the point furthest from the proximal tip). Note that since our model is a cloud of points, we will not be defining a curve, but rather a discrete set of nodes on the surface that appear to lie in a curve (Figure 11).

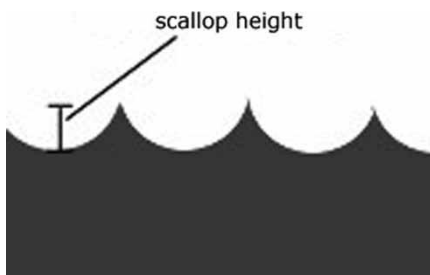


Figure 10. The circular cutting tool tip leaves ridges known as scallops. Scallop height is dependent on the amount of overlap of the cuts made by the tool.

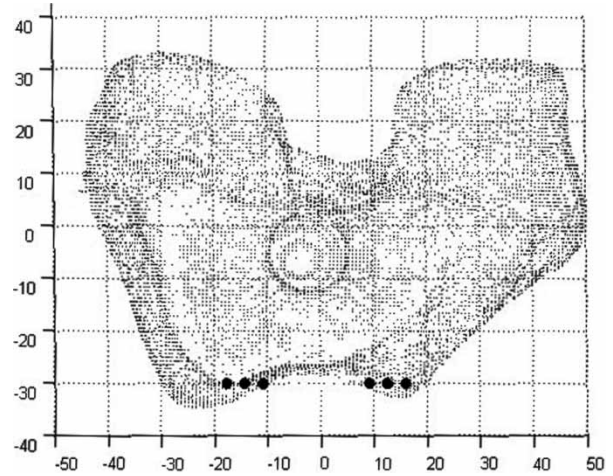


Figure 11. Step 1: Find the intersection of the start plane and knee model. Circles represent discrete points a set distance apart on the resulting intersection. Note that points on the intersection that fall outside the implant area are not shown.

2. Offset each resulting node on the intersection by an amount D along the surface in the direction of the other proximal/distal extremity, i.e., in a direction “orthogonal” to the start curve. D is determined by the desired size of the scallop height. The smaller the value of D , the smoother the resulting cut surface. Connecting the nodes at each iteration defines an offset curve in the surface (Figure 12).
3. Repeat step 2 until entire area has been swept out.
4. Remove parts of offset curves that fall outside the bone surface area where the implant will rest (Figure 13).
5. Reconnect parts of curves that cross the gap between boundaries on the proximal side of the implant (Figure 14).

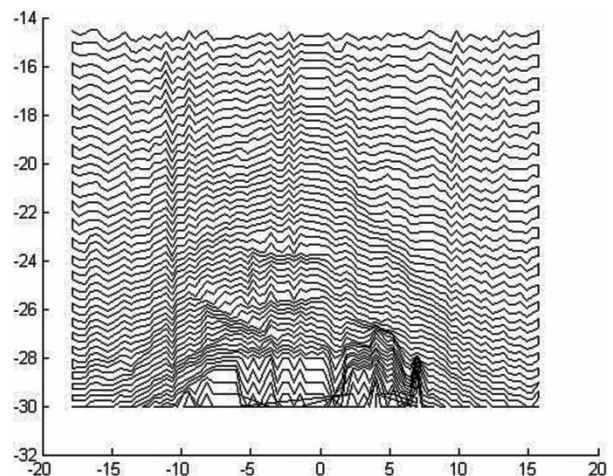


Figure 12. Steps 2–3: Sweep until entire the area containing the implant has been covered.

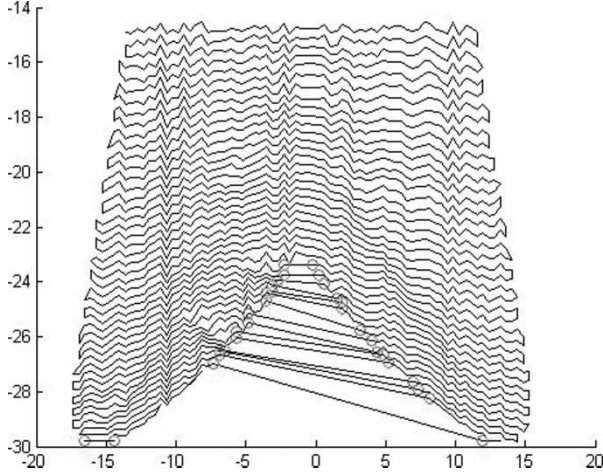


Figure 13. Pruning sweep lines for step 4 and identifying critical points for step 5. [Color version available online]

To ensure the feasibility of step 2, we present the mapping ϕ to take us from the bone surface to R^2 space. For convenience, we refer to the bone surface as an arbitrary surface U (Figure 15). ϕ is a diffeomorphic function that will provide us with the means to use a standard Euclidean metric.

Equations 3-6 define the mapping, and implicitly its inverse as well.

$$\phi: R^2 \rightarrow U \quad (3)$$

$$\phi(x,y) = (u,v) \in U \quad (4)$$

$$\phi \in C^\infty \quad (5)$$

$$\phi^{-1} \in C^\infty \quad (6)$$

While length along the surface projection is defined by the Euclidean two-norm, this is not the case for

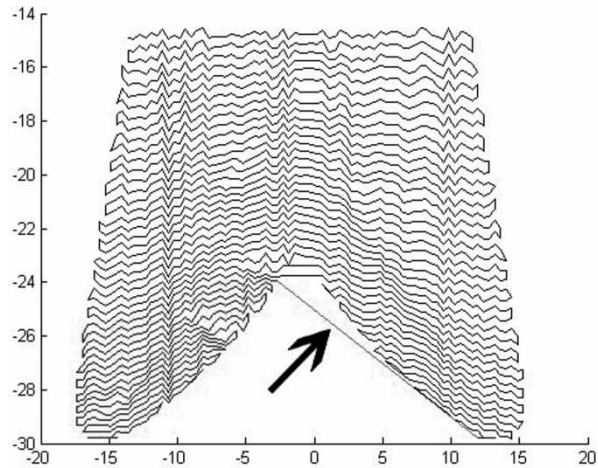


Figure 14. Step 5: Fix sweep lines that cross the negative area of the implant. Connect the two cells (as indicated by the arrow) for a single trajectory that covers the entire area to be milled. [Color version available online]

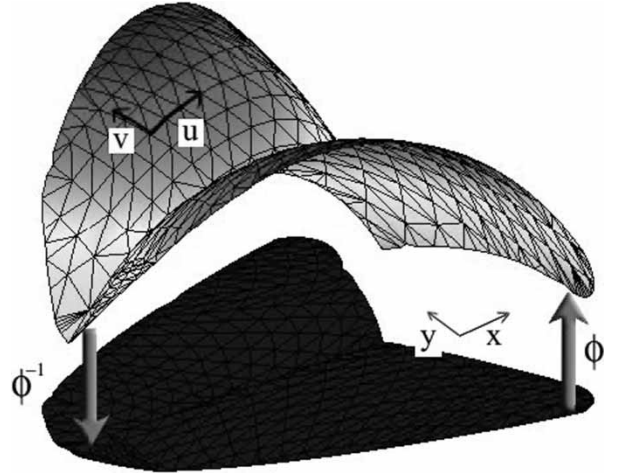


Figure 15. Mapping from R^2 to U . [Color version available online]

length along the surface.

$$l_{R^2} = \sqrt{(\Delta x)^2 + (\Delta y)^2} \quad (7)$$

For the purposes of offsetting the curve, we can use the ϕ . Given a known start-point of the curve, y_0 , we search for the y -coordinate in R^2 such that the following equation holds for our offset distance D .

$$\int_{y_0}^{y_1} \phi(x,y) dy = D \quad (8)$$

Potential field navigation

Once nodes along the surface for MBARS to visit are chosen, we can calculate “local navigation” using potential functions. Potential functions have already been widely used in mobile robot navigation. Khatib and others have provided examples for control of manipulators and mobile robots [16,17]. In summary, a potential function is a differentiable real valued function whose gradient defines a vector field. Navigation of a robot is done by treating the robot as a particle moving through the vector field. By making a goal have an attractive potential and obstacles a repulsive potential, virtual forces generated by the potential field direct a robot from start to goal.

We modeled our potential function after the attractive/repulsive model. Two of the following three forces affect the trajectory of the tip of the robot:

1. The target position provides an attractive force:

$$\vec{F}_a = K_a \cdot \frac{q_{\text{target}} - q_{\text{curr}}}{|q_{\text{target}} - q_{\text{curr}}|} \quad (9)$$

2. The bone surface provides an attractive force towards itself if the tip is outside a threshold:

$$\vec{F}_g = K_g \cdot \frac{q_{curr} - q_{close}}{|q_{curr} - q_{close}|} \quad (10)$$

3. The bone surface provides a repulsive force away from itself if the tip is inside the threshold:

$$\vec{F}_r = K_r \cdot \frac{q_{close} - q_{curr}}{|q_{close} - q_{curr}|} \quad (11)$$

In each case, q_{curr} is the current location of the robot, q_{target} is the target location, and q_{close} is the closest point on the knee to q_{curr} . K_a , K_g , and K_r are constants. Note that we do not simply create an attractive potential to an offset surface. This is done to allow $K_a \neq K_r$. The resulting force is then calculated:

$$\vec{F}_{net} = \begin{cases} F_a + F_g & \text{above threshold} \\ F_a + F_r & \text{below threshold} \end{cases} \quad (12)$$

We can now update the position of the robot:

$$q_{next} = q_{curr} + d_s \cdot F_{net} \quad (13)$$

where d_s is a constant step size. By making the step size constant, we ensure that the robot will take equal-size steps across the surface and consequently make equal-size cuts. This is our primary reason for choosing to use a potential function, as it is easy to ensure that the cuts remain uniform. The result is a trajectory that navigates from point to point at a fixed distance above the surface. We choose the fixed distance to be significantly smaller than the width of the burr head, so that the amount of bone being cut at one time is kept small. A step in the iterative process is illustrated in Figure 16.

By varying K_g , smoother trajectories can be formed (Figure 17). However, it is important to note that K_g must be significantly larger than the repelling constant, K_r , to ensure that the robot is constrained to the surface of the bone. In our implementation, the ratio of K_g to K_r was approximately 5 : 2.

Conclusion and future work

We have demonstrated the ability to generate a path for uniform coverage in a simulation. Our next step will be to test the system on the knee of a cadaver, and then use MBARS in actual surgery. We plan to integrate an interchangeable force probe, which,

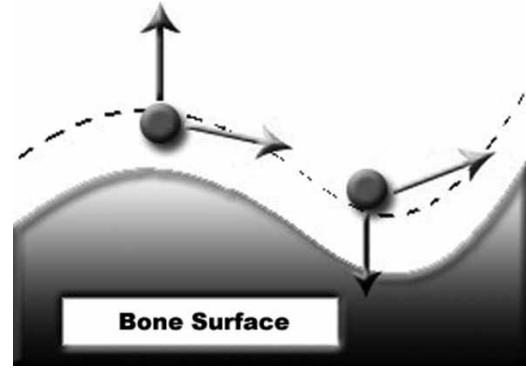


Figure 16. Typical trajectory as formed by virtual forces. The first position demonstrates the surface as a repulsive force, the second demonstrates it as an attractive force. [Color version available online]

taking the place of the bone burr, would be able to build an online model of the patient's knee. Again, this would also make the operating room procedure completely free of motion-tracking systems. Depending on the amount of processing required by this algorithm when integrated into current software, the system could potentially perform all computation on board and be computer-free as well. Once MBARS has been shown to be effective during a

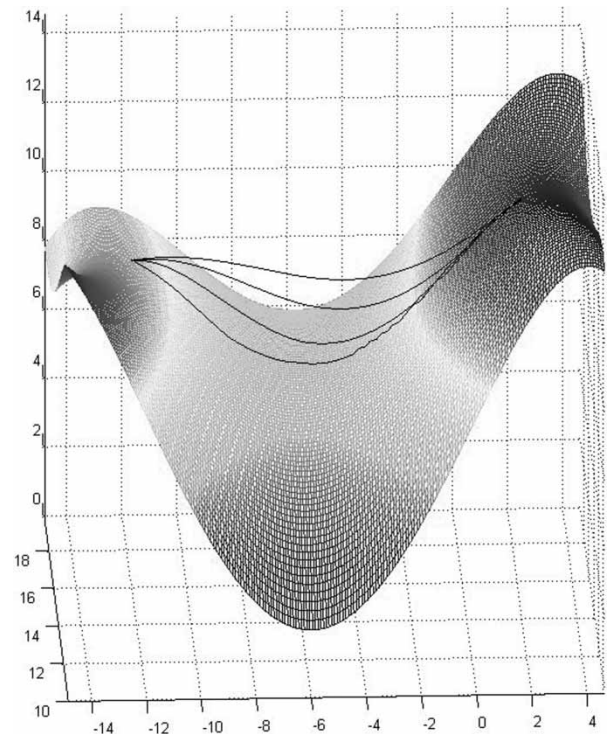


Figure 17. Simulated paths across a fourth-order polynomial. Curves further away from the surface correspond to smaller values of K_g . The polynomial was chosen using least squares to best fit the surface model points. [Color version available online]

PFJ surgery, we plan to use the same method on other orthopaedic procedures.

Acknowledgment

The first author gratefully acknowledges Brad Lisien for his continuing role in this project, as well as other members of both the Carnegie Mellon University Biorobotics Laboratory and the Institute for Computer Assisted Orthopaedic Surgery (ICAOS) at the Western Pennsylvania Hospital.

References

1. Kavoussi LR, Moore RG, Adams JB, Parin AW. Comparison of robotic versus human laparoscopic camera control. In: Proceedings of 2nd Annual International Symposium on Medical Robotics and Computer-Assisted Surgery (MRCAS '95), Baltimore, MD, November 1995. pp 284–287.
2. Kazanzides P, Mittelstands BD, Musits BL, Bargar WL, Zuhar JF, Williamson B, Cain PW, Cabon EJ. An integrated system for cementless hip replacement. *IEEE Eng Med Biol* 1995;14:307–312.
3. Marco A, Giachetti A, Gobbetti E, Zanetti G, Zorcolo A. A haptic model of a bone-cutting burr, 2003 <http://www.crs4.it/vic/data/papers/mmv-2003.pdf>
4. Harris SJ, Jakopec M, Hibberd RD, Cobb J, Davies BL. Interactive pre-operative selection of cutting constraints, and interactive force controlled knee surgery by a surgical robot. In: Wells WM, Colchester A, Delp S, editors: Proceedings of First International Conference on Medical Computing and Computer-Assisted Intervention (MICCAI '98), Cambridge, MA, October 1998. Lecture Notes in Computer Science Vol. 1496. Berlin: Springer; 1998. pp 996–1006.
5. Kienle TC III, Stulberg SD, Peshkin M, Quaid A, Lea J, Goswami A, Wu C. Total Knee Replacement: Computer-assisted surgical system uses a calibrated robot. *IEEE Eng Med Biol* 1995;14(3):301–306.
6. URS Ortho GmbH & Co. KG. CASPAR Orthopedics System. <http://www.ortomaquet.com>
7. Computer Motion, Inc. ZEUS Robotic Surgical System. <http://www.computermotion.com/zeus.html>
8. Chen MD, Wang T, Zhang QX, Zhang T, Tian ZM. A robotics system for stereotactic neurosurgery and its clinical application. Proceedings of the IEEE International Conference on Robotics and Automation, Leuven, Belgium, May 1998. pp 995–1000.
9. Dario P, Carrozza L, Lencioni B, Magnani S. A micro robotic system for colonoscopy. Proceedings of the IEEE International Conference on Robotics and Automation, Albuquerque, New Mexico, April, 1997. pp 1567–1572.
10. Merchant AC. LCS PFJ Prosthesis: Patellofemoral Joint Replacement. Depuy Orthopaedics, Inc., 2000.
11. Khodabandehloo K, Brett PN, Buckingham RO. Special-purpose actuators and architectures for surgery robots. In: Taylor RH, Lavallée S, Burdea GC, Mösger R, editors. Computer-Integrated Surgery: Technology and Clinical Applications. Cambridge, MA: The MIT Press; 1996. pp 263–274.
12. Merlet JP. Parallel Robots. Kluwer Academic Publishers, 2000. pp. 65–67.
13. Choset H, Lynch K, Hutchinson S, Kantor G, Burgard W, Kavraki L, Thrun S. Principles of Robot Motion: Theory, Algorithms, and Implementation. Cambridge, MA: The MIT Press; 2003.
14. Suresh KH, Yang DHC. Constant scallop height machining of free-form surfaces. *J Engineering for Industry* 1994;116:253–259.
15. Atkar PN, Choset H, Rizzi AA. Towards optimal coverage of 2-dimensional surfaces embedded in R^3 : choice of start curve. In: Proceedings of IEEE/RSJ Conference on Intelligent Robots and Systems (IROS), Las Vegas, NV, October 2003.
16. Khatib O. Real-time obstacle avoidance for manipulators and mobile robots. *Int J Robotics Res* 1986;5(1): 90–98.
17. Haddad H, Khatib M, Lacroix S, Chatila R. Reactive navigation in outdoor environments using potential fields. Proceedings of International Conference on Robotics and Automation, 1998, Leuven, Belgium, May 1998. pp 1232–1237.

